Spectroscopic investigation of gravitational lenses in the near-infrared

Eric Hsiao

March 31, 2004

Abstract. Five gravitational lens candidates were discovered spectroscopically in the Canadian Network for Observational Cosmology Field Galaxy Redshift Survey (CNOC2). The candidates were identified by discrepant emission lines that do not match any known features of the target galaxies. The lines were identified as either Lyα λ1216 or [O II] λ3727. Follow-up near-infrared spectra of three of the five candidates were reduced and examined here. The detection of [[O III]] λ5007 would unambiguously confirm that the discrepant line is a lensed Lyα. None of the near-infrared spectra for the three candidates showed definitive proof of the presence [[O III]] lines. The results suggest that the discrepant lines are not lensed Lyα. Future follow-up observations are needed to confirm the identities of the discrepant lines and the nature of the source galaxies.

1. Introduction

Gravitational lensing is a useful astrophysical tool. Lensing systems provide insights into the matter distributions of the deflector galaxies, the morphologies of the source galaxies and cosmological parameters.

A basic gravitational lens geometry is illustrated in Fig. 1 for point-like source and deflector. The point-mass approximation provides useful insights into a real gravitational lens system. The light path is deflected at an angle γ at the position of a massive deflector. From the weak-field limit of general relativity, the angle γ is given as a function of the distance r from the light path to the deflector:

$$\gamma(r) = \frac{4GM(r)}{c^2}\frac{1}{r},$$

where M is the mass of the deflector. From the geometry given in Fig. 1,

$$\gamma D_{LS} \simeq \alpha D_S .$$

The actual angular separation between the source and the deflector β can be expressed as

$$\beta = \theta - \alpha = \theta - \frac{D_{LS}}{D_L D_S}\frac{4GM}{c^2\theta}.$$

For the case where the source lies directly behind the deflector, $\beta = 0$, a complete ring of the source image, called an Einstein ring, is produced. The angle θ is defined as the Einstein radius θ_E:

$$\theta_E = \sqrt{\frac{4GM}{c^2}\frac{D_{LS}}{D_L D_S}}.$$

For the general case where $0 < \beta < \theta_E$, multiple images of the source galaxy are produced.

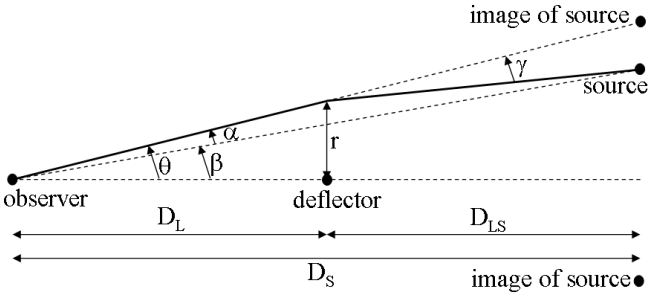

Fig. 1. A basic gravitational lens geometry for point-like source and deflector.

For a galaxy-galaxy lens system, the deflecting galaxy can be approximated by a singular isothermal sphere. The Einstein radius is then expressed as

$$\theta_E = 1.''455\sigma_{225}\frac{D_{LS}}{D_S},$$

where σ_{225} is the central dark-matter velocity dispersion in units of 225 $km\ s^{-1}$ (Narayan & Bartelmann 1999; Hall et al. 2000).

The probability that a bona-fide lens system is indeed present can be determined by the Einstein radius of the system. Provided that the surface density of faint, small galaxies at high redshift is large, significant number of strong galaxy-galaxy lens should exist (Miralda-Escude & Lehar 1992). Observations have shown that the surface density of high-redshift star-forming galaxies is indeed high (Steidel et al. 1996; Hu et al. 1998). The probability of lensing can then be considered as independent of source density. The cross section for lensing then scales as $\pi\theta_E^2$. The lensing geometry is described by the source and the deflector redshifts. The Einstein radius can be calculated for a presumed lensing geometry and

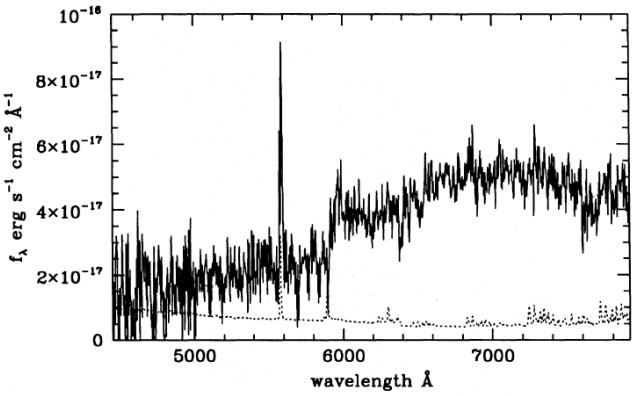

Fig. 2. The spectrum of the luminous early-type galaxy with a strong discrepant feature at 5588Å. (Warren et al. 1996)

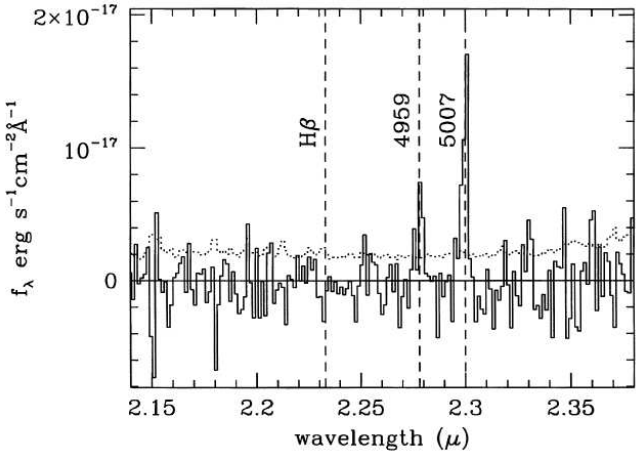

Fig. 3. Two lines [[O III]] $\lambda\lambda 4959, 5007$ of the source galaxy found in the near-infrared. (Warren et al. 1998)

used to estimate the probability of detecting such a lens. Lenses with smaller Einstein radii are much rarer than lenses with larger ones.

2. Spectroscopic lens search

The first galaxy-galaxy lens system discovered in a spectroscopic survey was presented by Warren et al. (1996). The deflector galaxy is a luminous early-type galaxy at a redshift of $z = 0.485$. A strong discrepant feature in the target spectrum does not match any known features of the deflector and is located at 5588Å (Fig. 2). Optical images taken of the same system suggested the presence of a gravitational lens. The discrepant line was then postulated to be from a lensed high-redshift source galaxy.

To unambiguously confirm the identity of the discrepant emission line, a second emission line from the source galaxy needed to be located. In 1998, the same group presented the results of their near-infrared spectroscopic observation of the same system (Warren et al. 1998). The lines of [O III] $\lambda\lambda 4959, 5007$ were detected near $2.3\mu m$, corresponding to the redshift of $z = 3.595$ (Fig. 3). The result of Warren et al. (1998) in the near-infrared secured the redshift of the source galaxy and identified the discrepant feature in the optical to be Lyα $\lambda 1216$.

The spectroscopic discovery of the galaxy-galaxy lens system by Warren et al. (1996) presented an alternative method of gravitational lens search. It has been shown by Steidel et al. (1996) that the surface density of high-redshift star-forming galaxies is high. The search strategy is then to find the optimal line-of-sight by identifying a population of effective deflector galaxies similar to the early-type deflector galaxy presented in Warren et al. (1996). Any source lying behind the deflectors must be significantly lensed. The spectrum of each of the deflector is then examined for a strong discrepant emission line which may be from the lensed and magnified images of a high-redshift source galaxy. Follow-up near-infrared spectroscopy is examined to locate a second emission feature from the source. The presence of [O III] in the near-infrared unambiguously identifies the discrepant line as Lyα and constraint the geometry of the system. The Einstein radius calculated using this lens geometry provides the lensing cross-section for the system.

There are many advantages of spectroscopic lens search over other methods. It is efficient as the surface density of high-redshift star-forming source galaxies was shown to be high (Steidel et al. 1996). The basic lensing geometry is determined upon discovery from the redshifts of source and deflector galaxies. The search method is independent of the morphology of the lens system, so that it is not affected by ambiguous morphologies that mimic the effects of lensing.

3. Method and observation

The goal of this project is to investigate in the near-infrared three of the five gravitational lens candidates presented in Hall et al. (2000). The properties of the three candidates are listed in Table 1. The candidates were discovered spectroscopically in the optical in the CNOC2 galaxy redshift survey.

The redshift of each of the target deflector galaxies were established from multiple spectral features above a set signal-to-noise ratio. Each lens candidate was identified by a strong discrepant emission line. The discrepant lines do not match any known features of the deflector galaxies and any known emission lines seen in local galaxies studied by (Sandage 1978). The the optical spectra of the three objects are shown in Fig. 4. The discrepant emission lines are marked with vertical lines. These discrepant lines are identified as either Lyα $\lambda 1216$ or [O II] $\lambda 3727$ by Hall et al. (2000).

If the discrepant lines are Lyα lines from high-redshift star-forming galaxies similar to the one presented by Warren et al. (1998), the [O III] doublets should be present in the near-infrared. The expected locations of the [O III] lines are listed in Table 1. The line $\lambda 5007$ is the stronger of the doublets. The detection of the [O III] doublets would secure the redshift of the source galaxy and constraint the lens geometry of the system.

The observations in the near-infrared were done at the European Southern Observatory's Very Large Telescope (VLT). The instrument used was the Infrared Spectrometer and Array Camera (ISAAC). The short-wavelength, medium-

object name	CNOC2 cat. number	$z_{deflector}$	observed λ of discrepant line	z_{source} (Lyα)	z_{source} (O II)	expected λ of O III (Lyα) λ5007	λ4959	θ_E (Lyα)	θ_E (O II)
J022336.4-000602	0223.191225	0.51142	5077	3.17764	0.36266	20917	20717	0.87	...
J144958.6+085447	1447.111371	0.39545	5274	3.33820	0.41503	21721	21513	0.76	0.04
J215057.9-055139	2148.150598	0.10589	6038	3.96509	0.61951	24860	24622	0.15	0.13

Table 1. The properties of the three lens candidates investigated. The wavelengths are in angstroms and the Einstein radii are in arcsec. (Hall et al. 2000).

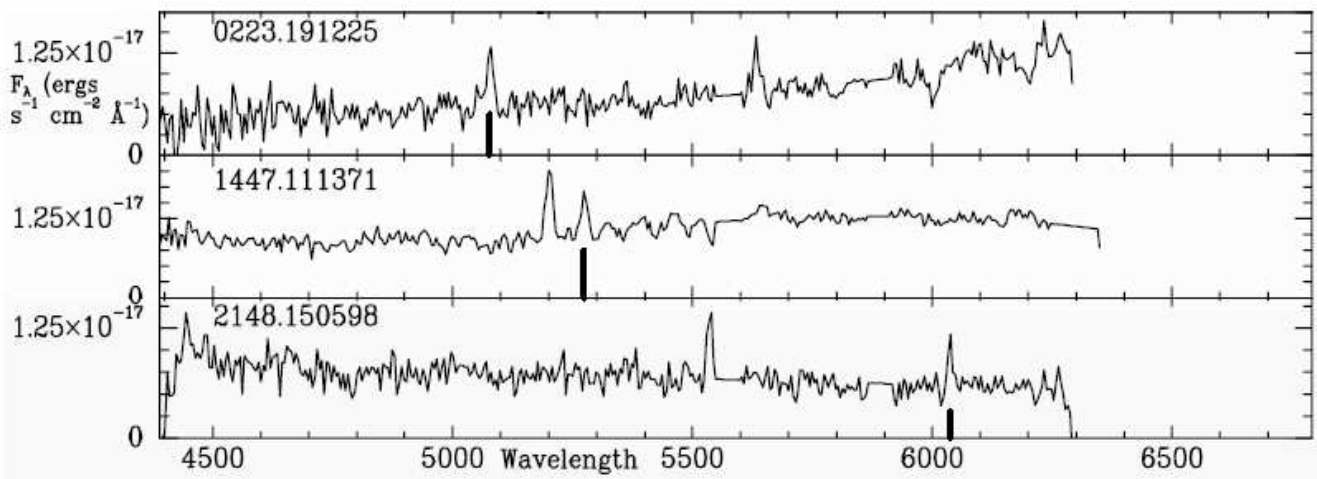

Fig. 4. Optical pectra of the three lens candidates. The discrepant lines are marked with vertical lines. The CNO2 catalog numbers were used to label the objects. Their corresponding IAU nomenclature object names are listed in Table 1 (Hall et al. 2000)

resolution spectroscopic mode (ISAAC SW MR) was employed. The gain of the detector is 4.5 electrons/ADU. The spectral regions covers the expected locations of the [[O III]] lines listed in Table 1.

The first two lens candidates, J022336.4-000602 and J144958.6+085447, were allotted eight hours of observing time including overhead at better than 1.0″ seeing. Each of the two targets had 24 exposures with 500 seconds of exposure time for each. The third target, J215057.9-055139, is observationally the most challenging. The expected location of the [[O III]] lines are at $\sim 2.5\mu m$, a spectral region of increasing thermal background. Including overhead, ten hours of observing time with better than 0.6″ seeing was required for this target. Over five nights, 130 250s-exposures were taken. Note that the number of exposures required is a lot higher than that of optical spectroscopy because of the strong background flux in the infrared region.

4. Reduction of near-infrared spectra

The most obvious difference between near-infrared spectra and optical spectra is the large background flux relative to the object in near-infrared spectra.

A commonly used technique to remove the background is known as ”nodding”. During the observation run, the object is ”nodded” along the slit between two positions along the spatial axis, a lower and an upper position. The frame that has the object in the lower position is called *A*, and the frame that has the object in the upper position is called *B*. A schematic of the nodding operation is shown in Fig. 5. The nod distance is the distance between the traces of frame *A* and frame *B*. A typical nod distance is about 400 pixels, corresponding to 60″. To ensure that each spectral trace lies on independent pixels, throw distances are introduced to the regions *A* and *B*. The spectra are taken with the target object lying at random positions within the thrown distance. A typical throw distance is about 120 pixels, corresponding to 18″.

The frames are taken in the sequence *ABBAAB*... and so on. When reducing the frames, consecutive pairs of frames *AB* or *BA* are subtracted. Because the object is taken at different positions along the spatial axis, the pairwise subtractions produce frames with reduced sky background and preserved object traces.

The reduction steps for the near-infrared spectra of this project are described as follows:

1. Flat-fielding The raw science frames were flat-fielded with a master flat frame for each observing night. A flat-fielded frame is shown in Fig. 6. For flat-fielding only removes the variations in pixel responses across a frame, sky lines still dominates the frame shown in Fig. 6. The spectral trace of the object at region *A* is barely visible at this point of the reduction.

2. Pairwise subtraction The nodding sequence was identified. Pairwise subtraction was performed for each *AB* or *BA* pair. A pairwise subtracted frame is included as Fig. 7. It shows the same region of the frame as Fig. 6. This is a $A - B$ frame. The trace of frame *A* is positive (white), and the trace of frame *B* is negative (black). Because both the *A* and *B* frames have ap-

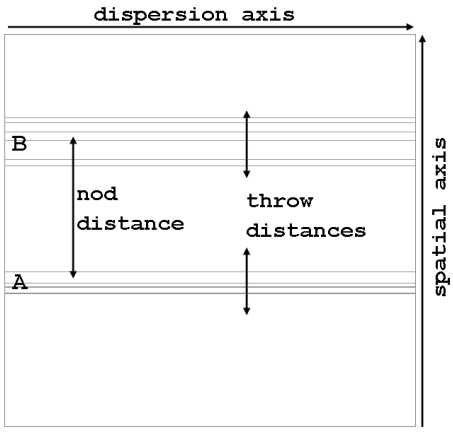

Fig. 5. A schematic of the nodding operation. The spectral traces lie at random positions within the throw distances of regions *A* and *B*.

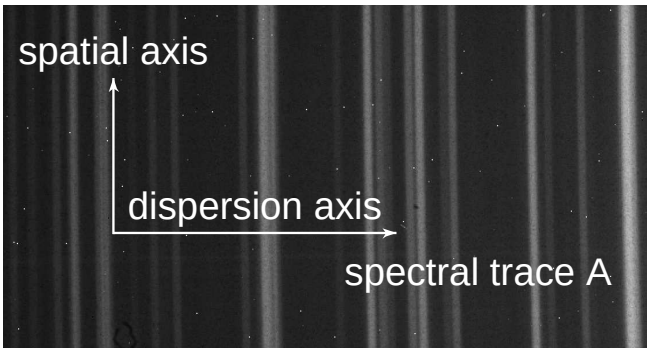

Fig. 6. A typical science frame after flat-fielding. The spectral trace of the object is dominated by the background flux and is barely visible.

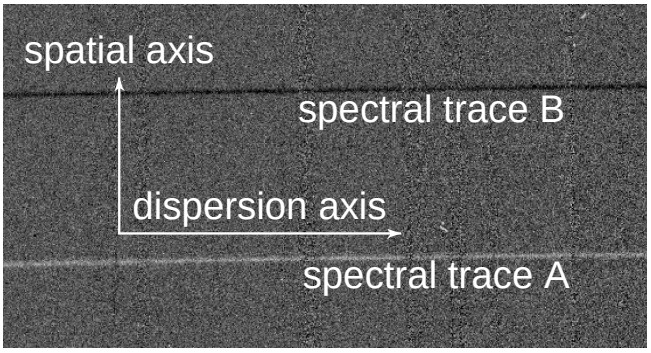

Fig. 7. A typical science frame after pairwise subtraction. The spectral traces from frame *A* and frame *B* are now clearly visible.

proximately the same sky background with the target spectral traces at different spatial positions, subtracting the frames removes most of the sky background and preserves the spectral traces (Fig. 6).

3. Isolating the traces Each pairwise subtracted frame is split into two trace frames, isolating the two spectral traces. Each negative trace was multiplied by -1 to make a positive trace.

The sky fluxes of an *AB* pair of science frames may not be exactly the same. Pairwise subtraction removes most of the sky flux but may over or under subtract. Fig. 8 illustrates the case

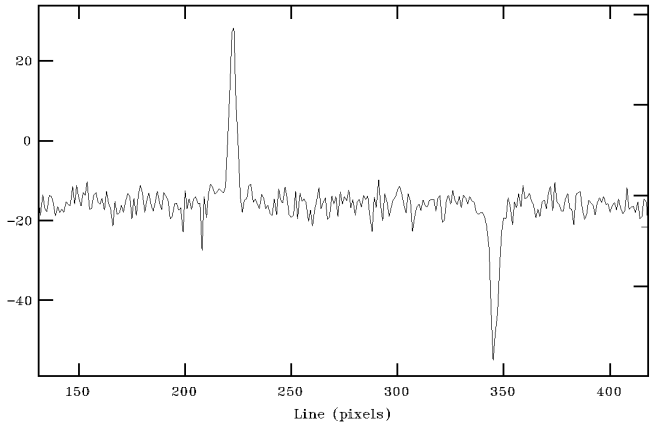

Fig. 8. An example of an over-subtracted sky by pairwise subtraction

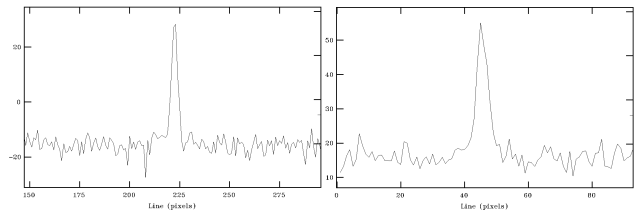

Fig. 9. Two isolated trace frames. The trace frame on the right contains the negative of the negative trace. Combining the negative of the negative trace and the positive trace remedies the over-subtraction of the sky and gives a sky residual of ~ 0.

where pairwise subtraction over-subtracts the sky. The residual sky level in Fig. 8 is at ~ -16 ADU. Fig 9 shows the two isolated trace frames. The trace frame on the right contains the negative of the negative trace. Multiplying the negative trace by -1 gives a sky residual of $\sim +16$ ADU. Combining the negative of the negative trace and the positive trace remedies the over-subtraction of the sky giving a sky residual of ~ 0.

4. Combining the traces The wavelength solutions varied from one observing night to another. In Fig. 10, the arc spectra from two consecutive observing nights were compared by subtraction. The location of a sky line varies as much as six pixels in the dispersion axis, corresponding to about 7.2Å. As a result, the traces from different observing nights needed to be combined independently even though they are of the same object.

Different rejection algorithms for combining the trace frames were also considered. The purpose of the rejection algorithms are to remove cosmic rays and bad pixels. Three IRAF rejection routines, “minmax”, “sigclip” and “avsigclip”, were tested with different combining operations. The “minmax” algorithm rejects the specified number of highest and lowest pixels. The “sigclip” and “avsigclip” methods reject pixels using sigma clipping algorithms.

The standard deviations of the combined frames using different rejection methods were compared in Fig. 11. With the “minmax” method, the noise of the combined frame is lower than with no rejection. The noise increases slightly as the num-

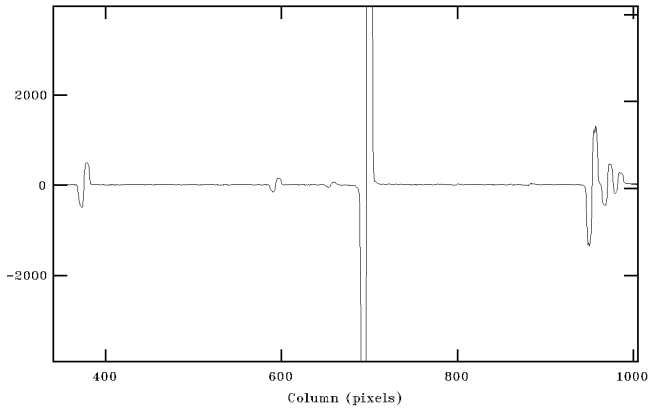

Fig. 10. The difference between arc frames from two consecutive nights. The comparison shows that the wavelength solutions vary from one observing night to another.

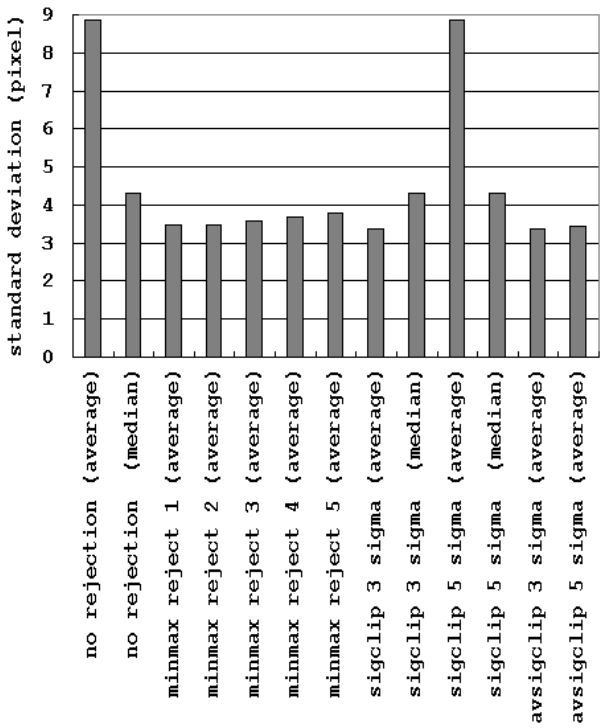

Fig. 11. Performances of different rejection algorithms. The type of combining operation is bracketed.

ber of high and low pixels rejected increases. The increase in noise is caused by the decrease in the number of pixels averaged, suggesting that rejecting one high and low pixel is sufficient.

Although some of the sigma clipping algorithms show lower noise in the combined frames, the resulting spectral traces are eroded near the sky lines. Fig. 12 shows an example of this. The combined frame on the left uses the "minmax" method, while the combined frame on the right uses the "sigclip" algorithm rejecting 3σ. It is clear that the "minmax" preserves the trace much better near a sky feature. Sigma clipping rejected some pixels of the sky flux before combining them, such that the sky removal operation described in step 3 did not work properly.

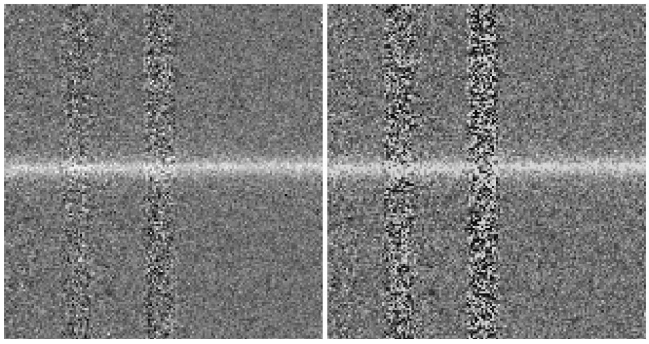

Fig. 12. An example of trace erosion by the sigma clipping algorithm. The combined frame on the left uses the "minmax" method, while the combined frame on the right uses the "sigclip" algorithm rejecting 3σ.

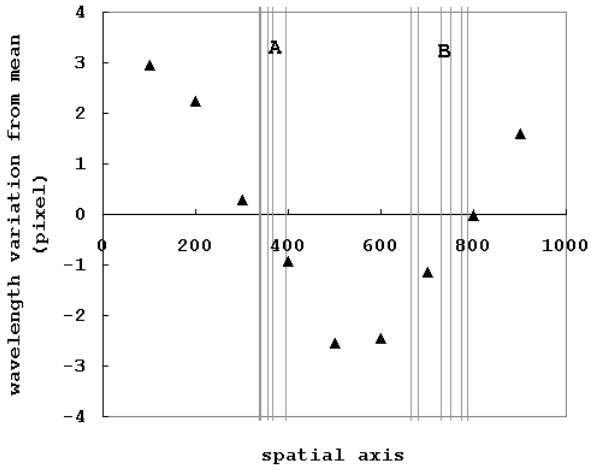

Fig. 13. The wavelength variation across the chip along the spatial axis.

The "minmax" method of rejecting the highest pixel and the lowest pixel is the optimal rejection method and was adopted for combining the spectral traces. The centres of the spectral traces were located. The trace frames were shifted in the spatial axis correspondingly and combined.

5. Extracting spectra The combined spectra were then extracted with different aperture sizes. If a lensed image of the source lies above or below the deflector galaxy along the slit, the source of the discrepant emission lines may be isolated by subtracting spectra extracted with different aperture sizes.

The arc spectra were extracted using the same extraction apertures as the object spectra, except for the centres of the apertures. Fig. 13 shows the wavelength variation across the chip along the spatial axis. The locations of the traces were plotted on the same graph. To minimize the effect of varying wavelength solutions along the spatial axis, a compromising centre for the arc aperture was chosen. For this case, the aperture was chosen to centre at pixel 350. The wavelength solutions at line 350 were verified to be approximately the same as the solutions at line 750.

6. Constructing the variance spectra The variance spectrum for each object and aperture size was then constructed. All the science frames were converted from ADU units to electron units. Each *AB* pair of frames were added to obtain the variance in each nodding subtraction operation. These frames were split and combined in exactly the same manner as described in the previous steps. The spectra were extracted using the same extraction apertures for the object frames, while background subtraction was omitted in the operation. The square root of the resulting variance frame gave the level of the noise in the continuum and higher noise at the locations of sky lines.

5. Results

The reduced spectra with their corresponding noise spectra are plotted in Fig. 15, Fig. 16 and Fig. 17. The expected locations of the stronger [O III] doublet are marked with vertical lines.

J022336.4-000602 The discrepant line cannot be a lensed [O II] line, since the source would have a lower redshift than the deflector. The discrepant line is most likely a lensed Lyα from the large Einstein radius. The spectrum in the near-infrared shows no strong features near the expected location of [O III]. There are several possibilities. The discrepant line in the optical is not a lensed Lyα and is a projected [O II] from a source in front of the presumed deflector galaxy. Another possibility is that the discrepant line is indeed a lensed Lyα. The source galaxy would then be of a different type from the one presented by Warren et al. (1998), such that [O III] lines of the source galaxy are weak or nonexistent.

J144958.6+085447 The near-infrared spectrum shows again no strong features near the expected location of [O III]. Again, one possibility is that the source galaxy is of different type from the one presented by Warren et al. (1998) and the discrepant line is indeed a Lyα. If the discrepant line is [O II], the Einstein radius would be very small (0.″04). This would make the system almost certainly not a gravitational lens. The discrepant line would most likely be from a projected source onto the deflector spectrum. The spectral profile (Fig. 14) of this target shows another object very close to the deflector galaxy. The discrepant line in the optical could come from this source. If this is the case, this target is not a gravitational lens system.

J215057.9-055139 This target was observationally the most challenging due to the high thermal background in the spectral region and it shows in the reduction. The sky features in the near-infrared spectrum could not be properly removed. The expected location of [O III] lies between two sky features and shows no presence of emission lines. The Einstein radii for both the Lyα or [O II] scenario are small. The discrepant line is then most likely a projected [O II].

6. Conclusion

The detection of [O III] doublets in the near-infrared would identify the discrepant emission lines in the optical as lensed Lyα. None of the three targets showed conclusive evidence of the presence of [O III] doublets. The intrinsic difficulties in working with near-infrared spectra and strong sky features lying near the expected location of [O III] have made the results less certain. The next step is to check if the discrepant lines are [O II] by resolving the doublets in the optical. If the the discrepant lines are identified as [O II], that almost certainly ruled the targets as gravitational lens systems because of the small Einstein radii. The proposal has been written on this premise. The results of this project and the proposed observations could help refine the spectroscopic lens search by distinguishing Lyα from [O II] doublets.

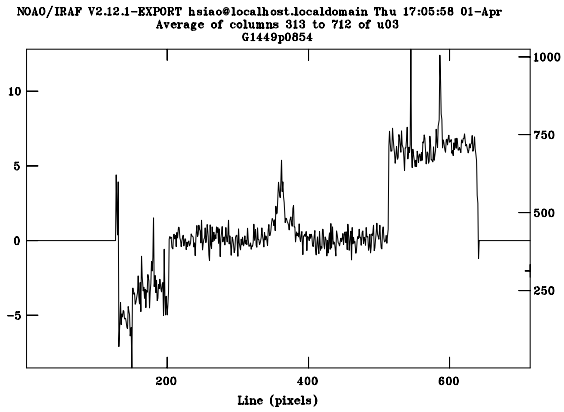

Fig. 14. The spectral profile of this target shows another object very close to the deflector galaxy.

References

Hall, P. B., Yee, H. K. C., Lin, H., et al. 2000, Spectroscopic Gravitational Lens Candidates in the CNOC2 Field Galaxy Redshift Survey, AJ, 120, 1660

Hu, E. M., Cowie, L. L., & McMahon, R. G. 1998, The Density of Ly alpha Emitters at Very High Redshift, ApJ, 502, L99+

Miralda-Escude, J. & Lehar, J. 1992, Optical rings - A large number of gravitational lenses?, MNRAS, 259, 31P

Narayan, R. & Bartelmann, M. 1999, Gravitational lensing, in Formation of Structure in the Universe, 360+

Sandage, A. 1978, Optical redshifts for 719 bright galaxies, AJ, 83, 904

Steidel, C. C., Giavalisco, M., Pettini, M., Dickinson, M., & Adelberger, K. L. 1996, Spectroscopic Confirmation of a Population of Normal Star-forming Galaxies at Redshifts Z > 3, ApJ, 462, L17+

Warren, S. J., Hewett, P. C., Lewis, G. F., et al. 1996, A candidate optical Einstein ring, MNRAS, 278, 139

Warren, S. J., Iovino, A., Hewett, P. C., & Shaver, P. A. 1998, Spectroscopy of the optical Einstein ring 0047-2808, MNRAS, 299, 1215

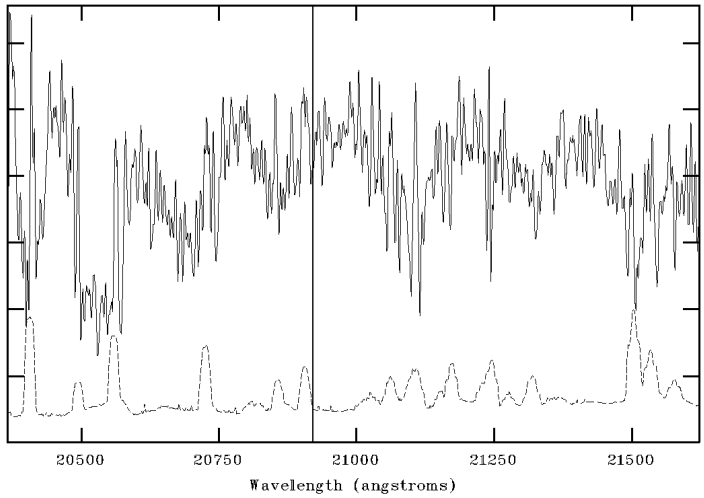

Fig. 15. Reduced spectrum of object J022336.4-000602. The expected location of O III is at 20917Å, for a source galaxy redshift of $z = 3.17764$

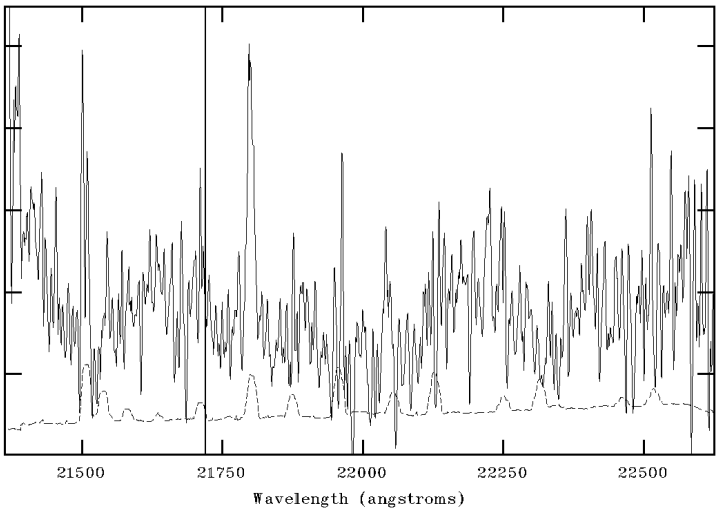

Fig. 16. Reduced spectrum of object J144958.6+085447. The expected location of O III is at 21721Å, for a source galaxy redshift of $z = 3.33820$

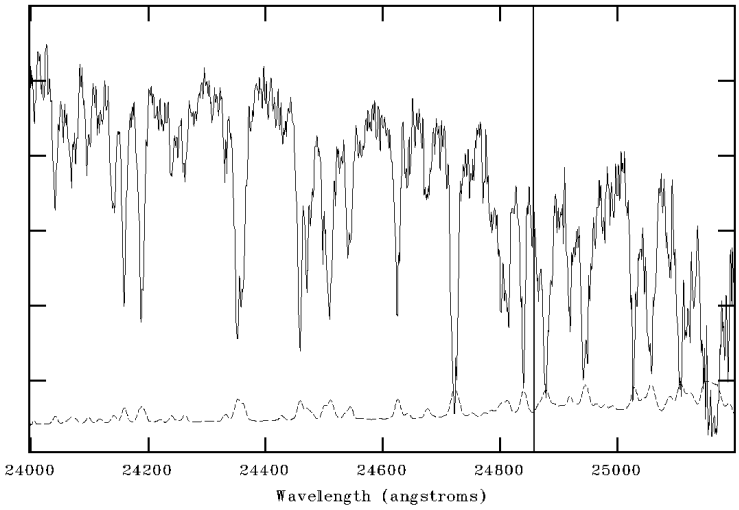

Fig. 17. Reduced spectrum of object J215057.9-055139. The expected location of O III is at 24860Å, for a source galaxy redshift of $z = 3.96509$

GEMINI OBSERVATORY

observing time request summary

Title:	**Spectrospcopic investigation of gravitational lens candidates from the CNOC2 field galaxy redshift survey**
Principal Investigator:	**Eric Hsiao**
PI institution:	University of Victoria, Department of Physics and Astronomy,PO Box 3055,Victoria,BC,V8W 3P6,Canada
PI status:	Other/Unspecified
PI phone / fax / e-mail:	250.721.7700 / 250.721.7715 / hsiao@uvic.ca
Co-investigators:	

Abstract: *The CNOC2 field galaxy redshift survey produced gravitational lens candidates. Each candidate was identified by a discrepant emission feature, presumably from a source galaxy, superposed to the target spectra. Follow-up near-infrared spectroscopy could not identify a second emission line to secure the redshift of the source galaxy. We propose to adequately resolve the emission feature to determine whether or not it is [O II] doublets. The GMOS-North detector with the B1200 grating would provide adequate resolving power to identify the discrepant emission features. A total of 8 hours of observing time, including overhead, are requested for three targets.*

Science Justification

The first galaxy-galaxy lens system discovered in a spectroscopic survey was presented by Warren et al. (1996). The system was identified by a strong discrepant emission line that does not match any known features of the deflector galaxy. In 1998, near-infrared observation of the same system was done and the [O III] doublets of the source galaxy were located. The [O III] doublets identified the discrepant line as Lyman alpha and secure the redshift of the source galaxy at z~3.

The spectroscopic discovery of the galaxy-galaxy lens system by Warren et al. (1998) presented an alternative method of gravitational lens search. It has been shown by Steidel et al. (1996) that the surface density of high-redshift star-forming galaxies is high. The search strategy is then to find the optimal line-of-sight by identifying a population of effective deflector galaxies. Any source lying behind the deflectors must be significantly lensed. The spectrum of each of the deflector is then examined for a strong discrepant emission line which may be from the lensed and magnified images of a high-redshift source galaxy. Follow-up near-infrared spectroscopy is then examined to locate a second emission feature from the source. The presence of [O III] doublets in the near-infrared unambiguously identify the discrepant line as Lyman

alpha and constraint the geometry of the system. The Einstein radius calculated using this lens geometry provides the lensing cross-section for the system.

There are many advantages of spectroscopic lens search over other methods. It is efficient as the surface density of high-redshift star-forming source galaxies were shown to be high. The basic lensing geometry is determined upon discovery from the redshifts of the source and deflector galaxies. The search method is independent of the morphology of the lens system, so that it is not affected by ambiguous morphologies that mimic the effects of lensing.

The CNOC2 field galaxy redshift survey produced five gravitational lens candidates (Hall et al. 2000). Each of the lens candidates was identified by a strong discrepant emission line (Fig. 1). The near-infrared spectra of three of the targets did not show conclusive proof of the presence of [O III] doublets. This result suggests a couple of possibilities. If the discrepant line in the optical is indeed Lyman alpha, it would mean that the source high-redshift galaxy is of a different type from the one presented in Warren et al. (1998). If a discrepant line is identified to be [O II], then the source galaxy of the discrepant line is at low redshift. It would also suggest that the target is most likely not a gravitational lens system, because of the small lensing cross-section in this configuration.

We presume that the discrepant emission line is [O II] and propose to resolve the doublets. If the [O II] doublets are resolved, there would be no doubt that the discrepant line is not a Lyman alpha. The source galaxy would be a low-redshift one. As a result, the first two targets would essentially be ruled out as lens systems. The last target could be a low-redshift lensed system. The results can help refine the spectroscopic lens search strategy. The discrepant lines discovered in the optical could be resolved such that the identity of the line can be narrowed down. Follow-up near-infrared spectroscopy then can search for a second emission line from the source to confirm the redshift of the source galaxy.

Technical Justification

The discrepant lines found in the lens candidates of CNOC2 galaxy redshift survey are presumed to be [O II] lines here. The [O II] doublets have rest-frame wavelengths of 3726 and 3729 angstroms with a flux ratio of 1:3.

The redshift of the source galaxies, if the discrepant lines are presumed to [O II], are listed in Table 1. The rest-frame wavelength separation is 3 angstroms and the redshifted separations would go up to 4-5 angstroms. The minimum resolving power required stays constant among the three targets at about 1240. To resolve the doublets properly, a resolving power of R=2500 is proposed. The GMOS B1200 grating provides an adequate resolving power of 2808 with a 0.75 arcsec slit width. The B1200 also provides good efficiency of at least 60% at the desired spectral region between 5000 to 6000 angstroms.

The line fluxes of the discrepant lines presented by Hall et al. (2000) are listed in Table 1. If a discrepant line is indeed [O II], the line flux observed by Hall et al. (2000)

is the integrated flux of the two lines. The goal here is to resolve the weaker of the two lines at 3726 angstroms. The line flux of the weaker line is approximately 25% of the integrated flux for a flux ratio of 1:3. The expected line flux for the first two targets is approximately 3*10^-17 ergs cm^-2 s^-1, and for the last target is 1*10^-17 ergs cm^-2 s^-1.

The water vapour content does not affect the spectral regions of these observations. The goal of the observations is only to detect the presence of the [O II] doublets, therefore there is no stringent demands on the observing conditions.

A signal-to-noise ratio of about 6 will adequately resolve the [O II] doublets. Each of the first two targets requires 7200s of on-target exposure, 25 minutes of telescope setup time and 96s of CCD readout time. The last target has a slightly lower line flux. It requires 9600s of on-target exposure and the same overhead as the first two targets. That makes a total of 8 hours of observing time for the three targets. The resulting signal-to-noise ratios determined by the integration time calculator are included as Fig. 2, Fig. 3 and Fig. 4 for the three targets.

Observation Details

Observation	**RA**	**Dec**	**Brightness**	**Total Time** *(including overheads)*
J022336.4-000602	2:23:36.4	-00:06:02	3.00e-17 ergs cm^-2 s^-1	146.6 minutes
GSC0469100923 (oiwfs)	2:23:30.341	-0:09:24.62	13.33 mag	separation 3.7
observing conditions: Global Default		resources:		
J144958.6+085447	14:49:58.6	+08:54:47	3.25e-17 ergs cm^-2 s^-1	146.6 minutes
GSC0091800865 (oiwfs)	14:50:08.904	8:54:43.63	11.36 mag	separation 2.55
observing conditions: Global Default		resources:		
J215057.9-055139	21:50:57.9	-05:51:39	0.135e-17 ergs cm^-2 s^-1	186.6 minutes
GSC0522200880 (oiwfs)	21:50:53.647	-5:53:18.17	13.56 mag	separation 1.96
observing conditions: Global Default		resources:		

Observing Conditions

Name	Image Quality	Sky Background	Water Vapor	Cloud Cover
Global Default	70%	50%	Any	50%

Scheduling Information:

Synchronous dates:

Optimal dates:

Impossible dates:

Additional Information

Keyword Category: Extra Galactic

Keywords: Gravitational lensing

Publications:

---

object name	CNOC2 cat. number	$z_{deflector}$	observed λ of discrepant line	z_{source} (O II)	expected $\Delta\lambda$ of O III	minimum R	integrated line flux	expected line flux of O II λ3726
J022336.4-000602	0223.191225	0.51142	5077	0.36266	4.09	1241	12.0	3.00
J144958.6+085447	1447.111371	0.39545	5274	0.41503	4.25	1241	13.0	3.25
J215057.9-055139	2148.150598	0.10589	6038	0.61951	4.86	1242	5.4	1.35

Table 1. The properties of the three lens candidates. The wavelengths are in angstroms. The line fluxes are in units of 10^{-17}ergs cm^{-2} s^{-1} (Hall et al. 2000).

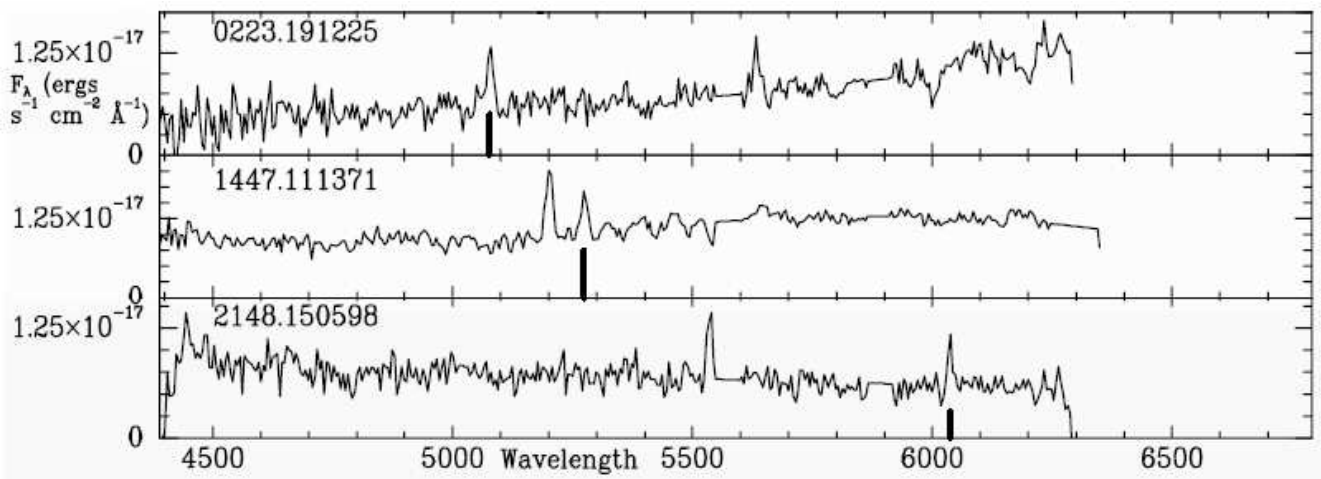

Fig. 1. Spectra of the three lens candidate. The discrepant lines are marked with vertical lines. The CNO2 catalog numbers were used to label the objects. Their corresponding IAU nomenclature object names are listed in Table 1 (Hall et al. 2000)

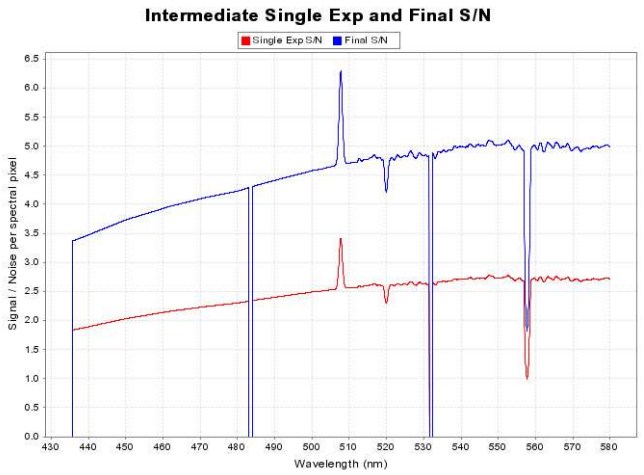

Fig. 2. The signal-to-noise ratio output from the integration time calculator for object J022336.4-000602.

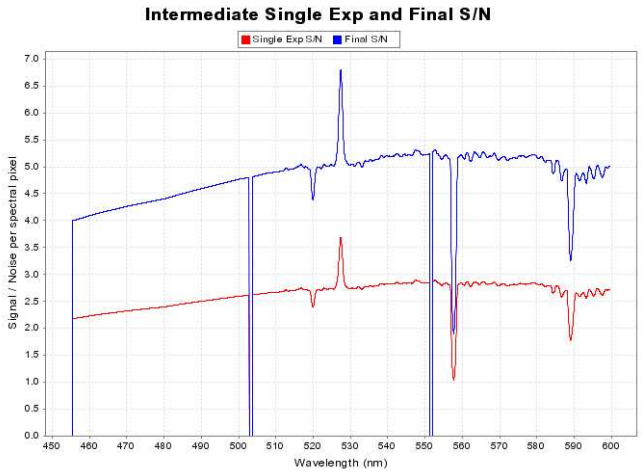

Fig. 3. The signal-to-noise ratio output from the integration time calculator for object J144958.6+085447.

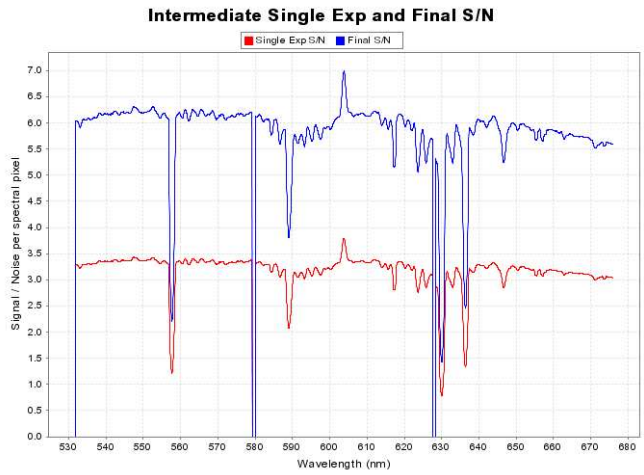

Fig. 4. The signal-to-noise ratio output from the integration time calculator for object J215057.9-055139.

References

Hall, P. B., Yee, H. K. C., Lin, H., et al. 2000, Spectroscopic Gravitational Lens Candidates in the CNOC2 Field Galaxy Redshift Survey, AJ, 120, 1660

Steidel, C. C., Giavalisco, M., Pettini, M., Dickinson, M., & Adelberger, K. L. 1996, Spectroscopic Confirmation of a Population of Normal Star-forming Galaxies at Redshifts Z > 3, ApJ, 462, L17+

Warren, S. J., Hewett, P. C., Lewis, G. F., et al. 1996, A candidate optical Einstein ring, MNRAS, 278, 139

Warren, S. J., Iovino, A., Hewett, P. C., & Shaver, P. A. 1998, Spectroscopy of the optical Einstein ring 0047-2808, MNRAS, 299, 1215